

White light-emitting diode daubed via $\text{CaSc}_2\text{O}_4:\text{Ho}^{3+}/\text{Yb}^{3+}$ nanocrystal sheets enclosed using SiO_2

Ha Thanh Tung¹, Dieu An Nguyen Thi²

¹Faculty of Basic Sciences, Vinh Long University of Technology Education, Vinh Long Province, Vietnam

²Faculty of Electrical Engineering Technology, Industrial University of Ho Chi Minh City, Ho Chi Minh City, Vietnam

Article Info

Article history:

Received Nov 1, 2022

Revised Nov 10, 2022

Accepted Dec 21, 2022

Keywords:

$\text{CaSc}_2\text{O}_4:\text{Ho}^{3+}/\text{Yb}^{3+}$

Downshifting

SiO_2

Ultraviolet–visible–near

infrared

White light-emitting diode

ABSTRACT

Our investigation assesses the downshifting (DS), periodicity up-transmutation as well as internal light consistency from phosphor samples of CaSc_2O_4 incorporated with $\text{Ho}^{3+}/\text{Yb}^{3+}$ along with up-conversion from CaY_2O_4 incorporated with $\text{Ho}^{3+}/\text{Yb}^{3+}$. These samples are created via precursor antecedent compound technique. The generation for the crystalline samples having orthorhombic stage is validated by the X-ray powder diffraction. The dispersal reflectance spectra exhibit several lines within the zones of ultraviolet–visible–near infrared (UV-vis-NIR), resulting from the ions of Ho^{3+} as well as Yb^{3+} . The optical band gap (E_g) results reach 5.69 and 5.58 eV, corresponding to $\text{CaSc}_2\text{O}_4:\text{Ho}^{3+}/\text{Yb}^{3+}$ and $\text{CaY}_2\text{O}_4:\text{Ho}^{3+}/\text{Yb}^{3+}$. The $\text{CaSc}_2\text{O}_4:\text{Ho}^{3+}/\text{Yb}^{3+}$ samples exhibit potent downshifting discharge in green hue when excited under 454 nm. $\text{CaSc}_2\text{O}_4:\text{Ho}^{3+}/\text{Yb}^{3+}$, as well as $\text{CaY}_2\text{O}_4:\text{Ho}^{3+}/\text{Yb}^{3+}$, exhibit potent discharges in green hue as well as near-infrared up-transmutation discharges in faint blue and red hues when excited under 980 nm. The spectrum hue clarity $-S_{gr}$ for $\text{CaSc}_2\text{O}_4:\text{Ho}^{3+}(1\%)/\text{Yb}^{3+}(5\%)$ reaches 0.78. The disparity in pumping force yields internal light consistency for said sample with the green discharge, being nonexistent in the $\text{CaY}_2\text{O}_4:\text{Ho}^{3+}(1\%)/\text{Yb}^{3+}(5\%)$ sample. As such, $\text{CaSc}_2\text{O}_4:\text{Ho}^{3+}/\text{Yb}^{3+}$ may prove useful when applied to up-transmutation apparatuses.

This is an open access article under the [CC BY-SA](https://creativecommons.org/licenses/by-sa/4.0/) license.



Corresponding Author:

Dieu An Nguyen Thi

Faculty of Electrical Engineering Technology, Industrial University of Ho Chi Minh City

No. 12 Nguyen Van Bao Street, Ho Chi Minh City, Vietnam

Email: nguyenthidieuan@iuh.edu.vn

1. INTRODUCTION

Phosphors incorporated with three-valence lanthanide appears to be a desirable option as they offer potent as well as distinctive power-states along with sharp f-f shifts caused by the electrons of 4f in the ions of Ln^{3+} being covered via occupied exterior shells of $6s^2$ as well as $5p^2$. With various power states having great multiplication as well as L-results [1], [2], the ions of lanthanide exhibit strengthened multi-modal luminescence, including up-transmutation, downshifting as well as quantum cleaving, which are determined by appropriate exciting radioactivity. Downshifting (DS) complies with the Stokes rule [3], [4], turning a small wavelength photon into big wavelength photon. It should be noted that the photon up-transmutation would be one non-linear light incident, creating discharge opposed to Stokes where the successive absorptivity for at least two photons with small power causes one luminescent discharge with strong power [5]. The up-transmutation luminescence (UTL) between near-infrared and observable states in lanthanide phosphors appears to be desirable for the flexibility they offer. Internal light consistency would be when the discharge strength avoids conforming to the behavior of surging or declining pumping force causing

hysteresis cycle [6]. The substances with light consistency can be employed for many optical apparatuses, including transistors as well as computers [7]. Different bases (fluorides, oxides, and phosphates) were thoroughly examined to gauge their luminescence. However, other substances such as scandate (Sc_2O_3) as well as yttrate (Y_2O_3) do not receive equal investigation. According to Tian's work, the luminescence from substances derived from scandium (Sc) were assessed, leading to findings of their applications, distinctive compared to substances with rare-earth constituents. In the case of hexagon-form $\text{NaScF}_4:\text{Yb}/\text{Er}$ nanoscopic granules yield potent UTL in red [8], distinctive compared to one from potent green discharge generated via variations for $\text{NaYF}_4:\text{Yb}/\text{Er}$. On the other hand, it is possible to generate the formational intersecting transmutation among orthorhombic $\text{KSc}_2\text{F}_7:\text{Yb}/\text{Er}$ and cube-shaped $\text{K}_2\text{NaScF}_6:\text{Yb}/\text{Er}$ nanoscopic particles via altering the chemical response [9]. In certain works [10]–[13], the formation alterations for various substances were assessed. CaSc_2O_4 , possessing orthorhombic CaFe_2O_4 formation as well as space group Pnam (62), offers certain benefits as it can act as one luminescent substance base that yields great chemical as well as heat consistency, small fluctuating periodicity, small chemical bindings (caused by tiny Sc^{3+} ion radius measured at 0.87 Å unlike other rare-earth components), small crystal field symmetry as well as potent crystal field strength. Bases with insignificant symmetry are known to yield one crystal field that possesses a greater number of bumpy constituents surrounding the doped ions, surpassing ones with significant symmetry [14], [15]. These constituents stimulate the electron joining among $4f$ power states and greater $4f5d$ settings, surging the chance of $f-f$ shifts for the doped ions. This will validate the extra benefit from the CaSc_2O_4 base with small symmetry. The potent crystal field may cause significant Stark cleaving for power states in said ions, resulting in greater power shift performance. On the other hand, the CaY_2O_4 base exhibit one small phonon periodicity at roughly 540 cm^{-1} . It will also lessen non-radioactive multi-phonon alleviation during up-transmutation activity [16].

This study will assess the formation attributes, DS as well as UTL in $\text{CaSc}_2\text{O}_4:\text{Ho}^{3+}/\text{Yb}^{3+}$ along with up-transmutation in $\text{CaY}_2\text{O}_4:\text{Ho}^{3+}/\text{Yb}^{3+}$ samples. The study will also look into the degradation kinetics for the distinctive discharges in the ions of Ho^{3+} under various Yb^{3+} content levels within the samples via employing Inokuti–Hirayama model (IH model), as well as observing DS and up-transmutation luminescence excited at 454 nm as well as 980 nm. Based on findings, $\text{CaSc}_2\text{O}_4:\text{Ho}^{3+}/\text{Yb}^{3+}$ exhibits greater up-transmutation strength, surpassing $\text{CaY}_2\text{O}_4:\text{Ho}^{3+}(1\%)/\text{Yb}^{3+}(5\%)$, along with internal light consistency.

2. METHOD

The study will involve creating $\text{CaSc}_2\text{O}_4:\text{Ho}^{3+}(1\%)/\text{Yb}^{3+}(x\%)$ with x values of 0, 5, 10, 20, 30 via employing the composite-derived preliminary compound technique that utilizes triethanolamine (TEA) in the form of compositing component [17]. In addition, $\text{CaY}_2\text{O}_4:\text{Ho}^{3+}(1\%)/\text{Yb}^{3+}(5\%)$ will be created via the same technique to compare characteristics. The creation process began with making the water-bearing component, which is $[\text{Sc}(\text{NO}_3)_3]$ (scandium nitrate) by putting $[\text{Sc}_2\text{O}_3]$ inside one beaker, then adding dual filtered H_2O as well as HNO_3 (nitric acid). Next, the blend was fired above one magnetic mixer under a temperature of $80\text{ }^\circ\text{C}$ within seven to eight hours, yielding limpid $[\text{Sc}(\text{NO}_3)_3]$. Next, the process involved adding various solid powders: $[\text{Ca}(\text{NO}_3)_2]$ (calcium nitrate), $[\text{Ho}(\text{NO}_3)_3]$ (holmium nitrate), $[\text{Yb}(\text{NO}_3)_3]$ (ytterbium nitrate) as well as $[\text{Y}(\text{NO}_3)_3]$ (yttrium nitrate) into dual filtered H_2O for the task of acquiring a metallic nitrates compound. Afterwards, we determined the proportions for $\text{Sc}(\text{NO}_3)_3$, $\text{Ca}(\text{NO}_3)_2$, as well as $\text{Ho}^{3+}/\text{Yb}^{3+}(\text{NO}_3)$, and created a merger between TEA and nitrate compound so that the entire ratio of metallic ion: TEA particle is sustained at 1:4. Initially, TEA was precipitated, caused by the created metallic hydroxides, accompanied by metallic ions. We dissolved the product, then introduced several HNO_3 droplets to acquire one limpid compound, with pH sustained under the value of 3 to 4. Next, the vaporization of the limpid compound TEA-derived metallic nitrate was carried out using one heated plate between the temperatures of $180\text{ }^\circ\text{C}$ and $200\text{ }^\circ\text{C}$, accompanied by continual mixing. Throughout the process, the nitrate ions produced in-situ oxidization condition for TEA, incompletely changing TEA hydroxyl groups to carboxylic acids. As water diminishes entirely, the nitrates degraded, exhibiting increased brown vapor from nitrogen dioxide, and yielding one preliminary powder in a great mass, which is black and organic-derived. Afterwards, we tempered this powder under a temperature of $1,200\text{ }^\circ\text{C}$ within two hours for the task of acquiring the desired phosphors. This entire creation process will also apply to $\text{CaY}_2\text{O}_4:\text{Ho}^{3+}(1\%)/\text{Yb}^{3+}(5\%)$.

Following the creation of the phosphor samples, the assessment of their attributes was carried out. Various tool was employed for the assessment task. Table 1 shows characteristics along with the tools used analyze them.

Table 1. Assessment of phosphor characteristics

Characteristics	Assessing tools
Phase purity	X-ray diffraction (XRD) inspection using Bruker AXS D8 automatic diffractometer having Cu-K α radioactivity ($\lambda=1.5418 \text{ \AA}$), under the angle scope of $20^\circ \leq 2\theta \leq 60^\circ$ subjected to 40 kilovolts as well as 40 milliamperes
Fluctuating groups	PerkinElmer IR spectrometer (FT-IR/FIR spectrometer Frontier) for observing Fourier transform infrared spectra (FTIR) in various phosphors
Ultraviolet-visible-near infrared (UV-Vis-NIR) spectra assuming dispersal reflectance state	PerkinElmer UV-Vis-NIR spectrometer (Lambda-750)
Up-transmutation discharge spectra	980 nm radiation generated by one diode laser along with an iHR320, Horiba Jobin Yvon, spectrometer accompanied by one photomultiplier tube
Steady-state and the time-resolved luminescent spectra	Subjecting the phosphors using an EKSPLA 10 ns pulsed optical parametric oscillator (OPO) laser, then acquiring the photoluminescence using Jobin-Yvon 320 spectrometer accompanied by one Hamamatsu NIR-extended photomultiplier linked with one Lecroy digital storage oscilloscope

3. RESULTS AND DISCUSSION

The non-radioactive power shift activities cause lower luminescence if the Yb³⁺ ion content surges, which is assessed by using the Inokuti-Hirayama model. With various shift characteristics assessed, it is possible to categorize the standard non-radioactive activities between the ions of Ln³⁺ into two types: if the prevalent interactivity between ions results from one multipolar activity concerning the giver as well as the receiver ions, the luminescent degradation intensity posterior to the laser pulse exciting process is determined as (1) [18]:

$$I(t) = I(0) \text{Exp} \left[-\frac{t}{\tau} - Q \left(\frac{t}{\tau} \right)^{3/S} \right] \quad (1)$$

$I(0)$ signifies the intensity under time t value of zero. τ signifies the internal duration for the giver level subjected to excitation. S signifies interactivity form among ions, assuming values of 6, 8, and 10 matching dipole-dipole, dipole-quadrupole, and quadrupole-quadrupole interactivities. Q will be determined as (2) [19]:

$$Q = \frac{4\pi}{3} T \left(1 - \frac{3}{S} \right) C (C_{DA} \tau)^{\frac{3}{S}} \quad (2)$$

T signifies the gamma function. C signifies the receiver ion content. C_{DA} signifies power shift between giver and receiver.

In case the prevalent interactivity results from reciprocation activity concerning the giver as well as the receiver ions, the luminescent degradation intensity correlating with time is determined as (3) [20]–[23]:

$$I(t) = I(0) \text{Exp} \left[-\frac{t}{\tau} - \gamma^{-3} Q_{Ex} g \left(e^{\gamma \frac{t}{\tau}} \right) \right] \quad (3)$$

γ signifies one constant corresponding to the critical shift range R_0 .

With the assessment for power shift activity, one predetermined internal duration for the ions of Ho³⁺ from the phosphor incorporated with only Ho³⁺ was utilized at 75 μs . On the other hand, according to Yu's work, surged doping content can alter the internal radioactive attributes for the functioning ions within certain matrices. For phosphors incorporated with Ho³⁺ and Yb³⁺, the content would be greater. If we have the fits for degradation arches for the Inotuki formula, the results for internal duration fluctuate in the 67–90 μs range, which signifies that the predetermined 75 μs result gained the phosphor with only Ho³⁺ would be a decent estimation. Under greater pumping force, the ions of Yb³⁺ generate dimer couples. The performance for power shift steadily diminishes, subsequently exhibiting consistent nature, then reaching a trivial level. The internal light consistency for the substances incorporated with Yb³⁺ exhibited Yb³⁺-Yb³⁺ dimers being generated, a result of collective interactivity among the ions of Yb³⁺ subjected excitation pointed out in Hehlen's work. According to Soni's work, the internal light consistency is caused by dimers' generation via dipole-dipole interactivity in the ions subjected to excitation. For collective interactivity, two ions of Yb³⁺ under the ground status concurrently assimilate two occurred photons under 980 nm, then reach the status of excitation. Afterwards, the ions mutually react to generate one couple-collective ion couple (dimer). As the pumping force surges, the Yb³⁺ ion content subjected to excitation surges, subsequently stimulating the collective interactivity among the Yb³⁺-Yb³⁺ ions subjected to excitation. This potent linear interactivity will augment the internal crystal field, causing internal light consistency. Throughout this study,

the investigating team kept track of this attribute via surging or diminishing the pumping force between 0.4 W and 2 W. The relationship between scattering coefficient and wavelength is depicted by various graphs seen in Figure 1. Under all percentages, the scattering coefficient would be inversely proportional to the wavelength, noticeably diminishing under greater wavelengths.

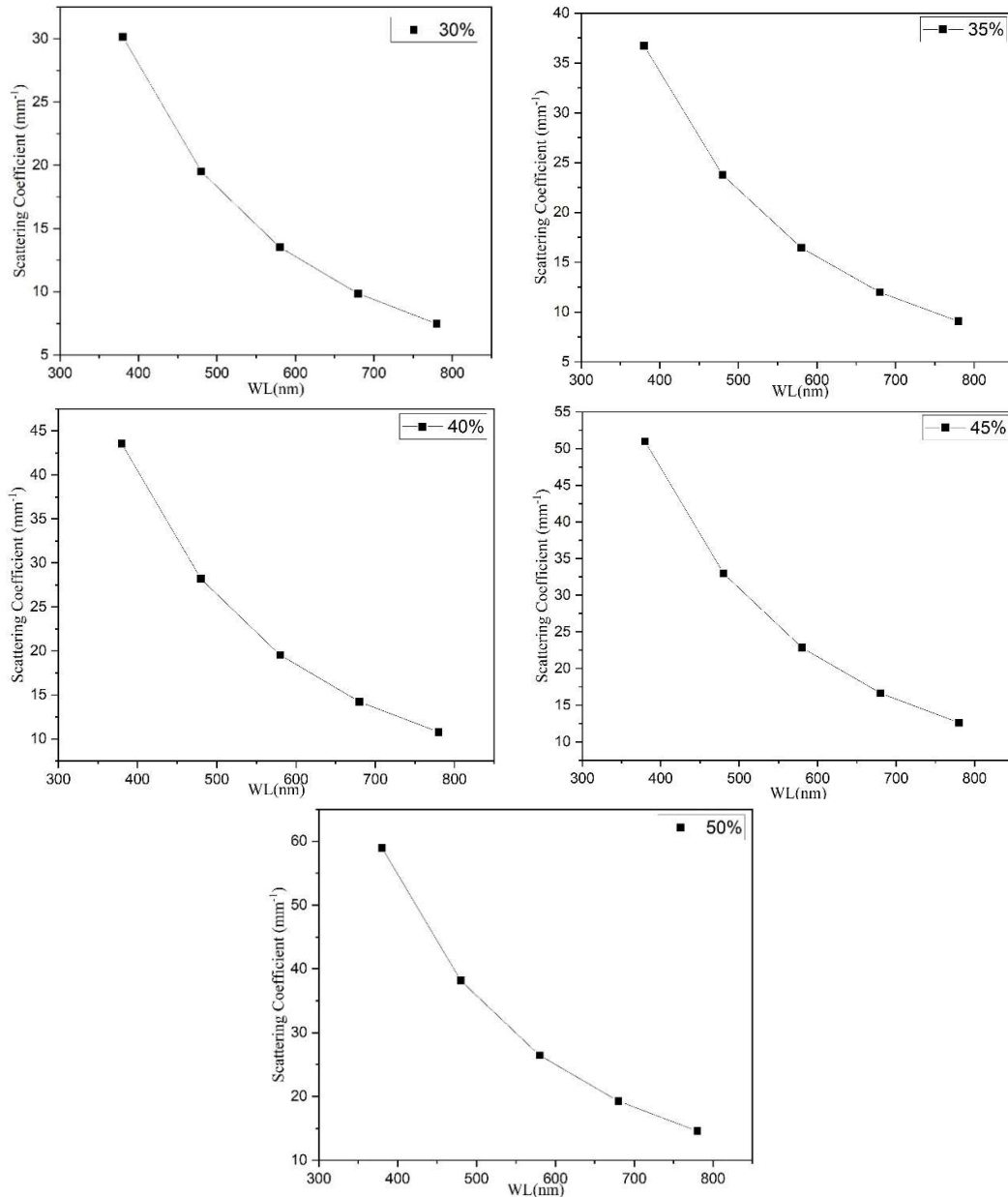


Figure 1. Scattering coefficient of $\text{CaSc}_2\text{O}_4:\text{Ho}^{3+}/\text{Yb}^{3+}@\text{SiO}_2$ as a function of varying phosphor concentration

Figure 2 depicts the correlation concerning the number density in a vol. of 1 mm³ as well as diameter measured in μm . Across all percentage levels, the dynamics exhibit similar patterns. In the range between 0.7 μm and 1 μm , the number density sees a substantial surge from 0 to 9,000,000, but plummets back its starting point under 1 μm and beyond.

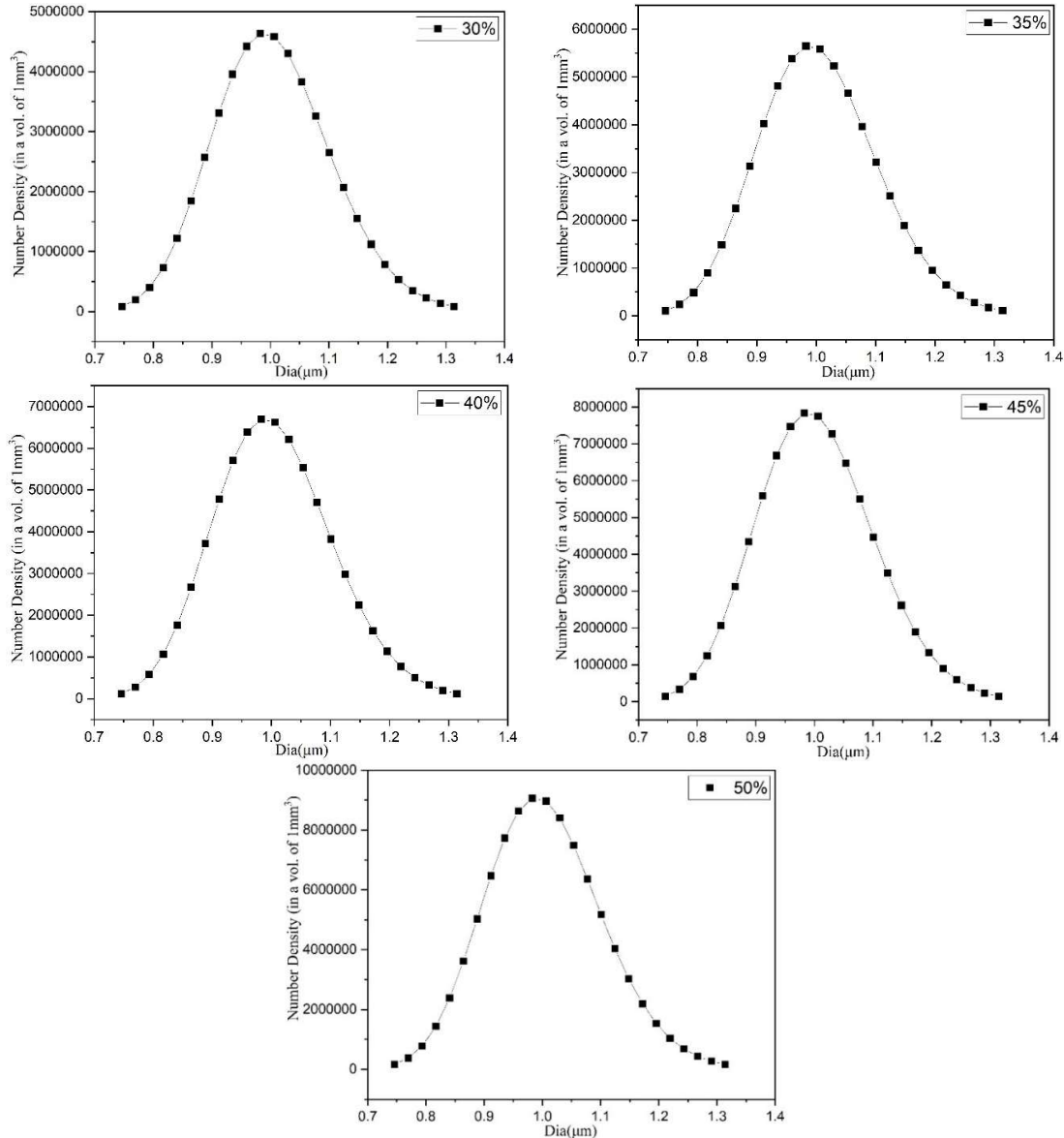


Figure 2. Number density of SrAlOCl:Bi³⁺@SiO₂ correlating with varying phosphor concentration

Figure 3 displays the dynamics between YGA:Ce contents and SiO₂ granule magnitude. The dynamics appears to be an inverse correlation, as YGA:Ce content wanes with increasing SiO₂ particle size. Figure 4 demonstrates the correlation between the granule magnitudes and correlated color temperature (CCT) levels. In the CCT range of 2,900 K to 3,050 K, the magnitude of granules will typically fluctuate between 35 nm to 50 nm. Notably, under greater CCTs of roughly 3,150 K and 3,200 K, the granules assume the sizes of 35 nm and 0 nm, respectively. Figure 5 depicts the interaction between the hue aberration and the granule magnitude of SiO₂. Under magnitude ranging from 0 to 30 wt.%, the hue aberration exhibits a substantial decline going from 230 K to mere 40 K. Going up to 35 wt.%, the hue aberration sees a sudden spike, plummets at 40 wt.% then surges back up under 50 wt.%. Figure 6 exhibits the correlation between the lumen in light-emitting diode (LED) and the granule magnitude of SiO₂. The lumen fluctuates between 0 and 30 wt.% but experiences a huge drop from 73 Ln to 70 Ln under 40 wt.%. Afterwards, the lumen exhibits a small surge under 50 wt.%.

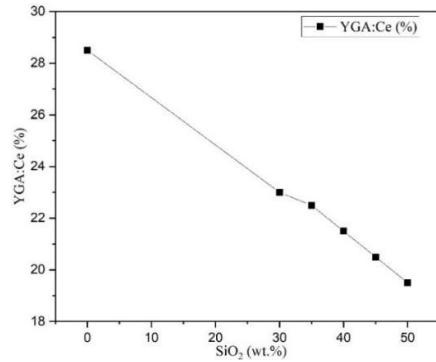


Figure 3. YGA:Ce decreases as a function of varying $\text{CaSc}_2\text{O}_4:\text{Ho}^{3+}/\text{Yb}^{3+}$ @ SiO_2 concentration

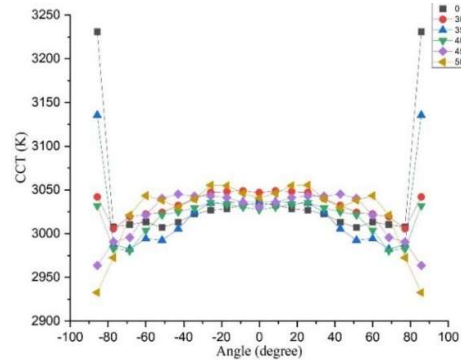


Figure 4. CCT changes as a function of varying $\text{SrAlOCl}:\text{Bi}^{3+}$ @ SiO_2 concentration

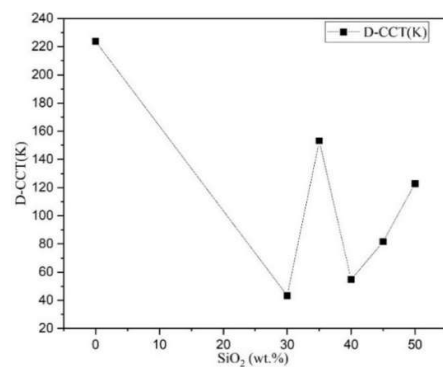


Figure 5. Examination of the hue aberration changing accordingly to SiO_2 granule magnitude

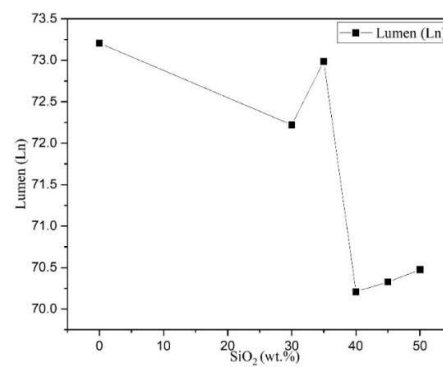


Figure 6. LED lumen alterations corresponding to changes in SiO_2 granule magnitude

Figures 7 and 8 depict correlation between the color rendering index (CRI) and color quality scale (CQS) in LED and the granule magnitude of SiO_2 . Similar interaction can be seen in both figures. From 0 to 30 wt.%, both CRI and CQS shows a decline in value, which is reversed when the magnitude is 35 wt.%. However, when approaching 40 wt.%, the two parameters suffer from a huge penalty, then steadily fall. Desirable illumination in the optical field would require maximal land equivalent ratio (LER) values accompanied by sublime he generation. Even if LER values are clearly determined, they cannot ensure “desirable” hue generation. As of today, the primary element used to gauge hue generation would be CRI [24], which is created through CIE 1965 and concerns the disparity between the hues from experimenting items lit via a testing light ray and the hues from items lit via a reference ray. Picking a reference ray would be essential for its role in assessing the genuine hues from items. To explicate CRI, unlimited quantity for reference rays would be employed, via considering the testing ray’s nature. Initially, the testing ray’s spectrum will be assessed alongside one black body radiator spectrum. The black body’s temperature that best fits the testing ray’s spectrum will be correlated color temperature–CCT–for the testing ray. If this element falls under 5,000 K, the reference ray employed to assess CRI would be the black body radiator for the element. In the case of values exceeding 5,000 K, one sun ray spectrum for the element would be employed. Fourteen distinctive testing hue patterns would be employed with eight of those employed to assess the universal CRI (R_a). The hues from testing items will be determined by the CIE 1964 uniform hue space, the CIE $U^*V^*W^*$ space [25], [26]. While CRI is meant for assessing the hue generation capability for illuminating rays, it is not an ideal element. Certain alternatives would be introduced, such as the universal CRI R_{96a} , which was never employed in reality. Eventually, another element derived from CIE criterion was introduced, which is CQS. Compared to CRI, this element employs a disparate hue space. For the task of assessing hue disparity judging the geometric range separating hue coordinates, the hue space must be employed in the most homogenous manner. CQS employs the CIE 1976 hue space, exhibiting greater homogeneity compared to the $U^*V^*W^*$ color space employed to assess the outdated CRI.

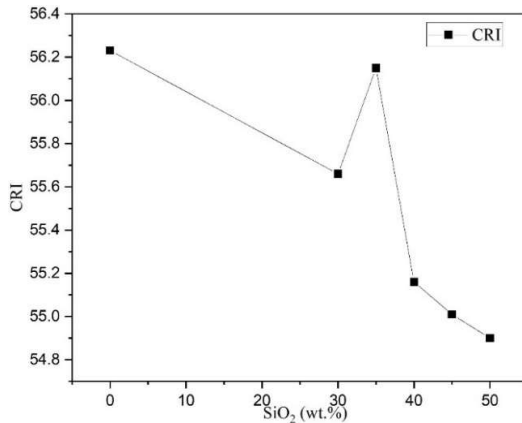


Figure 7. CRI performance as a function of varying SrAlOCl:Bi³⁺@SiO₂ concentration

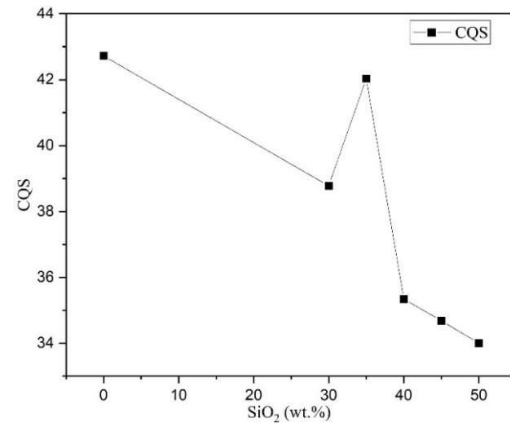


Figure 8. CQS values as a function of varying CaSc₂O₄:Ho³⁺/Yb³⁺@SiO₂ concentration

4. CONCLUSION

The samples of CaSc₂O₄:Ho³⁺/Yb³⁺ as well as CaY₂O₄:Ho³⁺/Yb³⁺ were created via the preliminary compound technique. The XRD behavior validate the structure for the orthorhombic stage in CaSc₂O₄ as well as CaY₂O₄. The UV-observable spectra for the samples of CaSc₂O₄:Ho³⁺/Yb³⁺ as well as CaY₂O₄:Ho³⁺/Yb³⁺ exhibit various assimilation apexes caused by the ions of Ho³⁺ as well as Yb³⁺. The FTIR spectra correlate with the extending fluctuations for the groups Ca–O, Sc–O as well as Y–O. The DS discharge for CaSc₂O₄:Ho³⁺/Yb³⁺ exhibit prevalent green discharge. We fitted the testing degradation arches to the Inokuti–Hirayama model for the task of assessing the interactivity among the doped ions within the samples. The untransmuted blue, green, red as well as NIR discharges for the ions of Ho³⁺ when excited under 980 nm existed with CaSc₂O₄:Ho³⁺/Yb³⁺ as well as CaY₂O₄:Ho³⁺/Yb³⁺. The spectrum hue clarity correlating with green hue reached 0.74 in the case of CaSc₂O₄:Ho³⁺/Yb³⁺. In addition, this sample generates internal light consistency in the case of green discharge. With the attributes above, CaSc₂O₄:Ho³⁺/Yb³⁺ can be employed in the form of a decent green discharger for photon-related sector as well as apparatuses with light consistency.




REFERENCES

- [1] H.-K. Shih, C.-N. Liu, W.-C. Cheng, and W.-H. Cheng, "High color rendering index of 94 in white LEDs employing novel CaAlSiN₃:Eu²⁺ and Lu₃Al₅O₁₂:Ce³⁺ co-doped phosphor-in-glass," *Optics Express*, vol. 28, no. 19, p. 28218, Sep. 2020, doi: 10.1364/OE.403410.
- [2] Y. Cheng and K. Sun, "Color modification of ZnGa₂O₄:Yb³⁺, Er³⁺, Tm³⁺ upconversion phosphors with the doping of Sn⁴⁺ and Ge⁴⁺ ions," *Applied Optics*, vol. 59, no. 24, p. 7313, Aug. 2020, doi: 10.1364/AO.399519.
- [3] A. Ali *et al.*, "Blue-laser-diode-based high CRI lighting and high-speed visible light communication using narrowband green/red-emitting composite phosphor film," *Applied Optics*, vol. 59, no. 17, p. 5197, Jun. 2020, doi: 10.1364/AO.392340.
- [4] Y. Fang *et al.*, "Giant enhancement of white light emission from Ca₉Ln(PO₄)₇:Eu²⁺, Mn²⁺ (Ln=La, Lu, Gd) phosphors achieved by remote aluminum reduction," *Optical Materials Express*, vol. 10, no. 5, p. 1306, May 2020, doi: 10.1364/OME.390069.
- [5] J. X. Yang, D. S. Li, G. Li, E. Y. B. Pun, and H. Lin, "Photon quantification in Ho³⁺/Yb³⁺ co-doped opto-thermal sensitive fluorotellurite glass phosphor," *Applied Optics*, vol. 59, no. 19, p. 5752, Jul. 2020, doi: 10.1364/AO.396393.
- [6] D. T. Tuyet *et al.*, "Deep red fluoride dots-in-nanoparticles for high color quality micro white light-emitting diodes," *Optics Express*, vol. 28, no. 18, p. 26189, Aug. 2020, doi: 10.1364/OE.400848.
- [7] J.-O. Kim, H.-S. Jo, and U.-C. Ryu, "Improving CRI and Scotopic-to-Photopic Ratio Simultaneously by Spectral Combinations of CCT-tunable LED Lighting Composed of Multi-chip LEDs," *Current Optics and Photonics*, vol. 4, no. 3, pp. 247–252, 2020, doi: 10.1364/COPP.4.000247.
- [8] D. Yan, S. Zhao, H. Wang, and Z. Zang, "Ultrapure and highly efficient green light emitting devices based on ligand-modified CsPbBr₃ quantum dots," *Photonics Research*, vol. 8, no. 7, p. 1086, Jul. 2020, doi: 10.1364/PRJ.391703.
- [9] L. Xie *et al.*, "Highly luminescent and stable lead-free cesium copper halide perovskite powders for UV-pumped phosphor-converted light-emitting diodes," *Photonics Research*, vol. 8, no. 6, p. 768, Jun. 2020, doi: 10.1364/PRJ.387707.
- [10] L. Li, Y. Zhou, F. Qin, Y. Zheng, and Z. Zhang, "On the Er³⁺ NIR photoluminescence at 800 nm," *Optics Express*, vol. 28, no. 3, p. 3995, Feb. 2020, doi: 10.1364/OE.386792.
- [11] H. E. A. Mohamed, K. Hkiri, M. Khenfouch, S. Dhlamini, M. Henini, and M. Maaza, "Optical properties of biosynthesized nanoscaled Eu₂O₃ for red luminescence applications," *Journal of the Optical Society of America A*, vol. 37, no. 11, p. C73, Nov. 2020, doi: 10.1364/JOSAA.396244.
- [12] N. C. Abd Rashid *et al.*, "Spectrophotometer with enhanced sensitivity for uric acid detection," *Chinese Optics Letters*, vol. 17, no. 8, p. 081701, 2019, doi: 10.3788/COL201917.081701.
- [13] J. Zhou and K. Qian, "Low-voltage wide-field-of-view lidar scanning system based on a MEMS mirror," *Applied Optics*, vol. 58, no. 5, p. A283, Feb. 2019, doi: 10.1364/AO.58.00A283.




- [14] J. Li, Y. Tang, Z. Li, X. Ding, L. Rao, and B. Yu, "Investigation of stability and optical performance of quantum-dot-based LEDs with methyl-terminated-PDMS-based liquid-type packaging structure," *Optics Letters*, vol. 44, no. 1, p. 90, Jan. 2019, doi: 10.1364/OL.44.000090.
- [15] T. Y. Orudzhev, S. G. Abdullaeva, and R. B. Dzhabbarov, "Increasing the extraction efficiency of a light-emitting diode using a pyramid-like phosphor layer," *Journal of Optical Technology*, vol. 86, no. 10, p. 671, Oct. 2019, doi: 10.1364/JOT.86.000671.
- [16] Y.-P. Chang *et al.*, "An advanced laser headlight module employing highly reliable glass phosphor," *Optics Express*, vol. 27, no. 3, p. 1808, Feb. 2019, doi: 10.1364/OE.27.001808.
- [17] T. Wei, W. Bo, C. Yan, C. Yeqing, L. Jun, and Z. Qingguang, "Single Pr³⁺-activated high-color-stability fluoride white-light phosphor for white-light-emitting diodes," *Optical Materials Express*, vol. 9, no. 1, p. 223, Jan. 2019, doi: 10.1364/OME.9.000223.
- [18] G. Simone, M. Gaiani, A. Ballabeni, and A. Rizzi, "Complex process of image color correction: a test of a target-based framework," *Journal of the Optical Society of America A*, vol. 38, no. 5, p. 663, May 2021, doi: 10.1364/JOSAA.414536.
- [19] S. Chen *et al.*, "Evaluation of regions suitable for vicarious calibration of ocean color satellite sensors in the South China Sea," *Optics Express*, vol. 29, no. 8, p. 11712, Apr. 2021, doi: 10.1364/OE.423108.
- [20] S. Jiao and J. Feng, "Image steganography with visual illusion," *Optics Express*, vol. 29, no. 10, p. 14282, May 2021, doi: 10.1364/OE.421398.
- [21] T. De Silva, E. Y. Chew, N. Hotaling, and C. A. Cukras, "Deep-learning based multi-modal retinal image registration for the longitudinal analysis of patients with age-related macular degeneration," *Biomedical Optics Express*, vol. 12, no. 1, p. 619, Jan. 2021, doi: 10.1364/BOE.408573.
- [22] Hsiao-Yi Lee, P. X. Le, and D. Q. A. Nguyen, "Selection of a Remote Phosphor Configuration to Enhance the Color Quality of White LEDs," *Current Optics and Photonics*, vol. 3, no. 1, pp. 78–85, 2019, doi: 10.25073/jaec.201934.249.
- [23] L. Wang, X. Wang, J. Kang, and C. P. Yue, "A 75-Mb/s RGB PAM-4 Visible Light Communication Transceiver System With Pre- and Post-Equalization," *Journal of Lightwave Technology*, vol. 39, no. 5, pp. 1381–1390, Mar. 2021, doi: 10.1109/JLT.2020.3034227.
- [24] R. Deeb, J. Van de Weijer, D. Muselet, M. Hebert, and A. Treneau, "Deep spectral reflectance and illuminant estimation from self-interreflections," *Journal of the Optical Society of America A*, vol. 36, no. 1, p. 105, Jan. 2019, doi: 10.1364/JOSAA.36.000105.
- [25] S. An, J. Li, X. Li, and Y. Su, "FTN SSB 16-QAM Signal Transmission and Direct Detection Based on Tomlinson-Harashima Precoding With Computed Coefficients," *Journal of Lightwave Technology*, vol. 39, no. 7, pp. 2059–2066, Apr. 2021, doi: 10.1109/JLT.2020.3046717.
- [26] R. H. Horng, S. Sinha, C. P. Lee, H. A. Feng, C. Y. Chung, and C. W. Tu, "Composite metal substrate for thin film AlGaInP LED applications," *Optics Express*, vol. 27, no. 8, p. A397, Apr. 2019, doi: 10.1364/OE.27.00A397.

BIOGRAPHIES OF AUTHORS



Ha Thanh Tung    received the Ph.D. degree in Physics from University of Science, Vietnam National University Ho Chi Minh City, Vietnam. He is working as a lecturer at the Faculty of Basic Sciences, Vinh Long University of Technology Education, Vietnam. His research interests focus on developing the patterned substrate with micro and nano-scale to apply for physical and chemical devices such as solar cells, OLED, and photoanode. He can be contacted at email: tunghtvlcrdt@gmail.com.



Dieu An Nguyen Thi    received a master of Electrical Engineering, HCMC University of Technology and Education, Vietnam. Currently, she is a lecturer at the Faculty of Electrical Engineering Technology, Industrial University of Ho Chi Minh City, Vietnam. Her research interests are theoretical physics and mathematical physics. She can be contacted at email: nguyenthidieuan@iuh.edu.vn.